Theoretical Study of Low-Lying Triplet States of Aniline

ARTICLE *in* THE JOURNAL OF PHYSICAL CHEMISTRY A · NOVEMBER 2005

Impact Factor: 2.69 · DOI: 10.1021/jp0533527 · Source: PubMed

Theoretical Study of Low-Lying Triplet States of Aniline

Xin-Juan Hou,[†] Phung Quan,[†] Tibor Höltzl,[†,‡] Tamás Veszprémi,[‡] and Minh Tho Nguyen*[,†]

Department of Chemistry, University of Leuven, Celestijnenlaan 200F, B-3001 Leuven, Belgium, and Department of Inorganic Chemistry, Budapest University of Technology and Economics, Gellért tér 4, H-1524 Budapest, Hungary

Received: June 21, 2005; In Final Form: September 16, 2005

Multireference complete active space self-consistent-field CASSCF(10,12)/ANO and second-order perturbation theory MS-CASPT2 calculations were performed to determine the vertical low-lying singlet and triplet states of aniline. The sequence of the seven lower lying triplet states is $T_1(1^3A')$, $T_2(1^3A'')$, $T_3(2^3A')$, $T_4(3^3A')$, $T_5(2^3A'')$, $T_6(4^3A')$, and $T_7(3^3A'')$. The $3^3A'$, $4^3A'$, and $3^3A''$ states are assigned as 3s, $3p_y$, and $3p_z$ Rydberg states, respectively, while other states correspond to $\pi^* \leftarrow \pi$ excitations. Both the T_1 and T_2 states are found to be below at the lowest-lying singlet S_1 ($1^1A''$) state. Geometry, vibrational modes, and electron distribution of the lowest lying T_1 state were determined using UB3LYP calculations. The vertical and adiabatic singlet−triplet energy gaps $\Delta E(S_0-T_1)$ amount to 3.7 and 3.5 ± 0.2 eV, respectively. In clear contrast with the S_0 state, the triplet aniline is no longer aromatic, and its protonation occurs preferentially at the ring *meta*-carbon site, with a proton affinity PA = 243 ± 3 kcal/mol.

1. Introduction

Photosynthesis is a fundamental process for life on Earth. This is a transformation in green plants and other organisms of visible light into organic chemical reactions. Information on the photosynthetic pigments can be obtained from their luminescence and phosphorescence. In this regard, knowledge on low-lying triplet electronic states is crucial when considering the photochemistry and photophysics.[1] For example in DNA bases, the dimerization of pyrimidinic thymine and cytosine derivatives has been found to occur after UV irradiation mediated by intersystem crossing from the excited singlet to the triplet state,[1,2] and recent calculated results suggested that the triplet state may also induce phototaumerization in Watson−Crick pairs.[3] The environmental sensitivity of the fluorescence and phosphorescence of phenylalanine, tryptophan, and tyrosine and their side chains is often examined when considering the macromolecular luminescence of natural peptides and proteins. Therefore, low-lying singlet and triplet states of toluene, aniline, and phenol can be studied as the simplest models of the proteins mentioned above, respectively. Knowledge of the various aspects of electronic spectra of the corresponding aromatic amino acids, in both low-spin and high-spin manifolds, has often been exploited to probe the photophysics and photochemistry of these proteins.[4]

The aniline singlet excited states have extensively been investigated using different spectroscopic and theoretical methods. Electronic spectra have been observed in gas phase,[5] aqueous solution,[6] perfluorohexane,[7] and crystal.[8] The vertical S_1 (lowest-lying singlet excited state) ← S_0 (singlet ground state) transition energy is identified at 34027−34029 cm^{-1} (4.219 eV).[9−11] The observation of an unfractionated aniline spectrum is in agreement with the high oscillator strength ($f = 0.028$) and the very large fluorescence quantum yield ($\Phi > 0.28$, depending on the vibronic level). This arises from the fact that a direct coupling between the S_1 state and the highly vibrationally excited states of S_0 is of higher order process of low efficiency. In addition, because of the relatively large energy gap between the S_1 and T_1 states (about 7200 cm^{-1}, 0.89 eV), the allowed first-order spin−orbit coupling between them is equally inefficient.[5] The fluorescence lifetime of aniline excited to the vibrationless S_1 state was reported as 7.8 ns.[12] Intersystem crossing is the main nonradiative process in the S_1 relaxation. The rate of intersystem crossing is as large as 8.2×10^7 s. The decay of the resulting triplet state is very fast; however, no phosphorescence was observed in the gas phase due to the rapid decay from lowest lying triplet state T_1 to S_0. Rydberg excited states of aniline and its derivatives have been located.[5,13] A novel band located between the first and second $\pi^* \leftarrow \pi$ transitions and centered at 37 104 cm^{-1} (4.62 eV above the S_0 and 0.38 eV above the S_1 state) has been observed.[13] This $^1A'$ state has been assigned to a 3s-Rydberg state.[14] While several studies on the singlet states of aniline have been reported, relatively less is known about its triplet states. The T_1 state of aniline has been probed using different spectroscopic methods. The values for $T_1 \leftarrow S_0$ electronic transition energy of aniline measured in phosphorescence in different media are quite consistent with each other, varying from 3.41 to 3.45 eV.[15,16] Scheps et al.[17] proposed that aniline in the T_1 state was bent as in the ground state with an angle of 31° between the CN bond and the NH_2 plane. Gee et al.[15] also proposed that aniline in the T_1 state has an out-of plane distortion that reduces the molecular symmetry point group to the C_s point group.

In this context, we set out to determine the structure and properties of the triplet states of the unsubstituted aniline, using quantum chemical methods. We hope that the obtained results could be helpful in understanding the electronic transitions of related aniline derivatives.

2. Details of Calculations

We used the density functional theory with the hybrid B3LYP functional[18] and the complete active space CASSCF[19] method

* To whom correspondence should be addressed. Fax: 32-16-327992. E-mail: minh.nguyen@chem.kuleuven.be.
[†] University of Leuven.
[‡] Budapest University of Technology and Economics.

10.1021/jp0533527 CCC: $30.25
Published on Web 10/25/2005

TABLE 1: Vertical Excitation Energies (*Tv*, in eV) and Nature of Singlet and Triplet Excited States of Aniline

state	transition	main configuration ($\|C\| > 0.3$)	Tv	SAC-CI[a]	expt[b]
X^1A'			0		
$1^1A'$ (S_2)	$\pi \rightarrow$ Ryd(s)	0.89(16a′−17a′)	4.85	4.53	4.60
$2^1A'$ (S_3)	$\pi \rightarrow \pi^*$	−0.77(16a′−20a′)	5.54	5.34	5.39
$3^1A'$ (S_5)	$\pi \rightarrow$ Ryd(s,p_z)	0.88(16a′−19a′)	5.99	6.06	
$4^1A'$ (S_7)	$\pi \rightarrow$ Ryd(p_x)	0.82(16a′−18a′)	6.38	6.26	
$1^1A''$ (S_1)	$\pi \rightarrow \pi^*$	0.74(16a′−11a″) − 0.44(9a″−20a′)	4.33	4.20	4.22
$2^1A''$ (S_4)	$\pi \rightarrow$ Ryd(p_z)	0.90(16a′−10a″)	5.92	5.57	
$3^1A''$ (S_6)	$\pi \rightarrow$ Ryd(s)	0.89(9a″−17a′)	6.28	6.39	
41A″	$\pi \rightarrow \pi^*$	−0.53(9a″−20a′) − 0.45(15a′−11a″) +0.37(16a′-11a″) + 0.37(9a″−11a′)	6.92	6.62	6.40
$1^3A'$ (T_1)	$\pi \rightarrow \pi^*$	−0.83(16a′−20a′) + 0.37(9a″−11a″)	3.74		
$2^3A'$ (T_3)	$\pi \rightarrow \pi^*$	0.75(9a″−11a″) + 0.35(16a′−17a′)	4.40		
$3^3A'$ (T_4)	$\pi \rightarrow$ Ryd(s)	0.78(16a′−17a′) − 0.37(9a″−11a″)	4.60		
$4^3A'$ (T_6)	$\pi \rightarrow$ Ryd(p_y)	0.81(16a′−19a′) − 0.32(16a′−17a′)	5.86		
$1^3A''$ (T_2)	$\pi \rightarrow \pi^*$	0.94(16a′−11a″)	3.82		
$2^3A''$ (T_5)	$\pi \rightarrow \pi^*$	−0.91(9a″−20a′)	5.31		
$3^3A''$ (T_7)	$\pi \rightarrow$ Ryd(p_z)	0.90(16a′−10a″)	5.88		
43A″	$\pi \rightarrow$ Ryd(s)	−0.76(9a″−16a′) − 0.47(9a″−17a′)	6.22		

[a] Values taken from ref 14. [b]The vertical excitation energy values for S_1 state are taken from ref 13, and other values are taken from ref 5.

to optimize the geometries. Subsequently, second-order multiconfigurational perturbation theory (CASPT2)[20] and multistate second-order perturbation theory (MS-CASPT2)[21] methods were applied to determine excitation energies. For open-shell systems, the unrestricted formalism UB3LYP was used with 6-311++G-(d,p) basis set. Atomic natural orbital (ANO-S) basis sets of C([10s6p3d]/3s2p1d), N([10s6p3d]/3s2p1d), and H([7s]/2s)[22] were used for the CASSCF and CASPT2 calculations.

To describe correctly not only valence states but also the low-energy Rydberg states, we also generated Rydberg basis functions. On the basis of the B3LYP-optimized geometry, we first performed CASSCF calculation for aniline with one electron removed to determine the center of charge. Then the generated Rydberg basis functions were added to the center of charge. Earlier SAC/SAC-CI calculation results[14] indicated that there is no d-Rydberg orbital involved for the excitation up the 18th singlet excited state. By checking the RASSCF orbitals, we found that 3d-Rydberg basis functions have indeed no contributions to the orbitals ranging from LUMO to LUMO+10, which means that there are no d-Rydberg excited states existed for the low-lying singlet and triplet states considered. Therefore, we only considered 3s- and 3p-Rydberg orbitals in CASSCF calculations for the low-lying singlet and triplet excited states. The Rydberg 3s and 3p functions with exponents of 0.024624 and 0.042335, respectively, were used. Then MS-CASPT2 energies were constructed to evaluate the vertical excitation energies of four roots of lowest lying singlet and triplet excited states in both a′ and a″ symmetries. In the CASSCF/CASPT2 calculations for vertical excitation energies, 10 electrons were chosen for variable occupancy in an active space of 12 orbitals including 8a′ and 4a″ orbitals.

Although the vibrational frequencies were obtained with both UB3LYP/6-311++G(d,p) and CASSCF methods, the normal vibrational modes were analyzed using UB3LYP results. The gas-phase proton affinity (PA) of aniline in the T_1 state was calculated by PA = E(aniline) − E(protonated aniline), where E denotes the total electronic energy of the excited state corrected by the corresponding zero-point energies (ZPEs). Geometries and frequencies of aniline protonated at different positions were optimized at the UB3LYP/6-311++G(d,p) level. The electron distribution in the high-spin state was also analyzed by employing different approaches.

All the calculations were performed using Gaussian 03 suit of program[23] and MOLCAS 6.0 quantum-chemistry software.[24] The same threshold and shift were used in all CASSCF/CASPT2 calculations of the singlet and triplet states.

3. Results and Discussion

3.1. Low-Lying Excited States of Aniline. The vertical singlet−singlet and singlet−triplet energy gaps are calculated as the differences in total energies of the ground-state S_0 and relevant excited states at the ground singlet optimized geometry. The adiabatic energy gap is evaluated as the difference between the energies of both singlet and triplet states at their respective relaxed geometries. The vertical energy gaps of aniline calculated by CASPT2 methods are summarized in Table 1, whereas the adiabatic excitation energies for the T_1 state of aniline calculated by CASPT2 and UB3LYP methods are shown in Table 2. A correlation diagram of the vertical energies of S_1 and T_1 states of benzene and a series of monosubstituted derivatives is depicted in Figure 1.

The dominant orbital configuration for the S_0 state of aniline (X^1A') is ...$(15a')^2$ $(9a'')^2(16a')^2$ $(17a')^0(10a'')^0$. Despite the a′ labeling due to the C_s symmetry plane, all the three HOMO's are of π-character. Therefore, the lowest lying excitations are due to $\pi^* \leftarrow \pi$ transitions. A novel band located between the first and second $\pi^* \leftarrow \pi$ transitions and centered at 37104 cm^{-1} (4.62 eV above the S_0 and 0.38 eV above the S_1 state) has been assigned to a 3s-Rydberg state.[13,14] Our multistate perturbation theory calculations using the optimized S_0 geometry also concur with this, and the calculated excitation energy is consistent very well with the experimental result (Table 1).

Our MS-CASPT2 calculations predict the sequence of seven lowest lying triplet states as follows: $1^3A'$, $1^3A''$, $2^3A'$, $3^3A'$, $2^3A''$, $4^3A'$, $3^3A''$. The dominant configuration for each high-spin excited state can be described as a single-electron excitation. Accordingly, the above states arise essentially from the single excitations from the 16a′ to 20a′ orbital ($1^3A'$), 16a′ to 11a″ ($1^3A''$), 9a″ to 11a″ ($2^3A'$), 16a′ to 17a′ ($3^3A'$), 9a″ to 20a′ ($2^3A''$), 16a′ to 19a′ ($4^3A'$), and 16a′ to 10a″ ($3^3A''$). While the first three lower lying triplet states and the T_5 state correspond to $\pi^* \leftarrow \pi$ excitation, the T_4, T_6, and T_7 excited states correspond to excitation from π orbital to 3s-, $3p_y$-, and $3p_z$-Rydberg orbitals, respectively.

The CASPT2 value of 4.33 eV for the vertical $S_1 \leftarrow S_0$ transition is quite close to the experimental result of 4.22 eV.[9−11] Within the expected accuracy of the present calculations, namely ±0.3 eV, it is confirmed that the triplet T_1 (3.74 eV) and T_2

TABLE 2: Adiabatic Excitation Energies (in eV) for the T_1 State of Aniline in CASPT2/ANO-S[a] and UB3LYP/6-311++G(d,p) Calculations

		excitation[b]	CASSCF	CASPT2	(U)B3LYP/6-311++G(d,p)	expt[c]
aniline	S_0	...$(16a')^2(9a'')^2$	0 (−285.859 79)	0 (−286.665 95)	0 (−287.687 74)	
	T_1	$16a' \rightarrow 17a'$	3.39	3.59	3.45	3.41−3.45

[a] CASSCF and CASPT2 calculations were performed at the CASSCF-optimized geometries. The values in parentheses are the total energies in au. [b] The dominant configuration in the CASSCF wave function. [c] Taken from refs 15 and16.

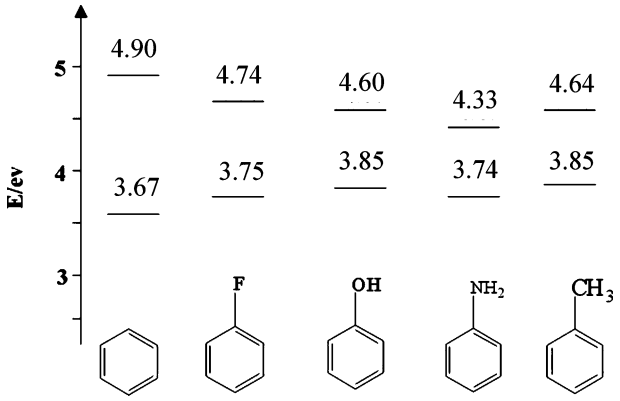

Figure 1. Vertical energies of the S_1 and T_1 states for benzene and its monosubstituted derivatives. See ref 26 for fluorobenzene, ref 27 for phenol and toluene, and refs 28 and 29 for benzene.

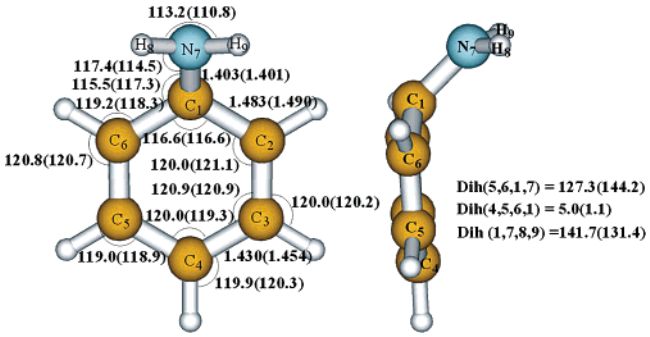

Figure 2. Selected (U)B3LYP/6-311++G(d,p) geometrical parameters of aniline in the lowest lying triplet state. Values given in parentheses are calculated at the CASSCF/ANO-S level. Bond distances are given in Å and angles in deg.

TABLE 3: Calculated Hyperfine Coupling Constant Values (in G) and Spin Density (in e) for Aniline in the T_1 State Using the (U)B3LYP Method[a]

	Hfcc's[c]	
atoms[b]	6-311++G(d,p)	EPR-II
C_1	28.5	31.9
C_2	3.6	4.3
C_3	−2.2	−2.0
C_4	8.0	9.3
N_7	13.0	13.8
H_{10}	−0.7	−0.5
H_{11}	2.4	2.4
H_{12}	−7.0	−7.4
H_8	0.8	1.2

[a] Using the optimized (U)B3LYP/6-311++G(d,p) structure. [b] See Figure 2 for atom numbering. [c] Spin densities (Fermi contact terms) are obtained at the (U)B3LYP/ 6-311++G(d,p) level, with two basis sets.

(3.82 eV) states are lower in energy than the singlet S_1 state (4.33 eV; cf. Table 1). Because the experimental energy gap from the S_0 state to the T_1 state was reported to be 3.41−3.45 eV,[15,16] it appears that this value corresponds to an adiabatic singlet−triplet gap, and the vertical excitation energy is larger than this value. This indicates that the earlier CASSCF vertical value of 3.30 eV[25] is underestimated.

The calculated energy gap of 0.6 eV between S_1 and T_1 states of aniline compares well with the experimental value of 0.75 eV (6104 cm^{-1} in Ar matrix[17]). Figure 1 shows that the energy differences between S_1 and T_1 states of substituted benzenes are in the range 0.66−0.99 eV,[26,27] which is obviously smaller than the corresponding value of benzene (1.23 eV[28,29]). Thus, a large substituent effect occurs on this property.

Results given in Table 2 indicate that the UB3LYP value for the singlet−triplet gap is closer to the experimental counterpart than that from the more sophisticated CASPT2 method. It is in fact well-known that adiabatic singlet−triplet energy separations of aromatic compounds can be accurately predicted by DFT computations.[30,31] It is the result of a rather subtle balance between different effects in the UB3LYP, and it is hard to say if this comes from an intrinsic property of the functional or from a cancellation of errors. On the other hand, the CASPT2 calculation also depends on the choice of the active spaces and basis sets.

Here, with combination of both the CASPT2 and B3LYP results, the calculated $T_1 \leftarrow S_0$ energy gap of aniline of about 3.5 eV is consistent with the experimental value of 3.41−3.45 eV, determined by phosphorescence measurements in different media[15,16] (27 547 cm^{-1} in cyclohexane at 77 K and 27 851 cm^{-1} in argon matrices).

3.2. Molecular Geometry of T_1 Aniline. Figure 2 displays selected geometrical parameters of aniline in the T_1 state optimized at both UB3LYP/6-311++G(d,p) and CASSCF(10,12)/ANO-S levels. For the purpose of comparison, the corresponding calculated geometry for the ground state is shown in the electronic Supporting Information (Figure 1S).

Intrinsic difference in the electronic structure of both ground and triplet states provides a basis for analyzing of the singlet−triplet transition. There is in general no significant difference between the two sets of geometric values. Indeed, the CASSCF values for the bond distances and angles are very similar to the corresponding UB3LYP values. Only the dihedral angle values calculated by CASSCF are larger as compared to the corresponding UB3LYP values. We only discuss the UB3LYP results in the following section. The molecular skeleton in the T_1 state keeps the C_s point group, but the amino group is strongly perturbed and more bent than in the ground state. Although the ring is slightly distorted, it possesses a quinoidal form. Relative to the S_0 state, the C−N distance of 1.403 Å is marginally compressed. The NH_2 group is obviously distorted from the phenyl ring undergoing a substantial out-of-plane motion (52°). The dihedral angles of HNH_7C_1 and HHN_7C_1 in the T_1 state are 124.3 and 141.7°, respectively, and the angle between CN and the HNH group amounts to 35°, which supports the suggestion of Scheps et al.[17] put forward from their experimental data that this angle is about 31°. The barrier to inversion of the T_1 state is about 2.0 kcal/mol, which is marginally larger than that of 1.5 kcal/mol for the S_0 counterpart.

The hyperfine coupling constant values and spin density for aniline in the T_1 state are shown in Table 3. The UB3LYP/6-311++G(d,p) and UB3LYP/EPR-II methods predicted very

TABLE 4: (U)B3LYP/6-311++G(3df,2p) Harmonic Vibrational Frequencies (cm^{-1}), Infrared Intensities, Assignment, and PED for the Normal Modes of the T_1 Aniline[a]

no.	freq.	sym.	int.	assignment, PED (%; ≥10%)
1	109	A′	7.6	δ_{3rg} (46) + δ_{2rg} (26) − $\gamma(C_1N_7)$ (12)
2	220	A″	19.3	δ_{1rg} (55) + δ_{4rg} (22)
3	311	A″	0.4	δ_{4rg} (41) + $\beta(C_1N_7)$ (39)
4	320	A′	9.5	$\gamma(C_1N_7)$ (47) + δ_{3rg} (33)
5	428	A″	2.1	δ_{4rg} (53) − $\beta(C_1N_7)$ (19)
6	502	A′	7.7	β_{2rg} (71)
7	563	A′	112.8	δ_{2rg} (37) − $\gamma(H_8H_{14})$ (24)
8	578	A″	0.7	β_{3rg} (70)
9	589	A′	167.6	$\gamma(H_8H_{14})$ (56) + δ_{2rg} (16)
10	680	A′	26.9	δ_{2rg} (41) − $\gamma(C_4H)$ (38)
11	714	A″	3.8	$\gamma(C_6H)$ (36) − $\gamma(C_2H)$ (36)
12	771	A′	7.5	$\nu(C_1C_2)$ (26) + $\nu(C_1C_6)$ (26) − $\gamma(C_4H)$ (11) + $\nu(C_1N_7)$ (11)
13	787	A′	15.2	$\gamma(C_6H)$ (26) + $\gamma(C_2H)$ (26) − $\gamma(C_4H)$ (17)
14	905	A″	0.2	$\gamma(C_5H)$ (23) − $\gamma(C_3H)$ (23)
15	941	A′	9.8	$\nu(C_4C_5)$ (24) + $\nu(C_3C_4)$ (24) − β_{1rg} (14) −$\gamma(C_3H)$ (12)
16	957	A′	0.2	β_{1rg} (71)
17	972	A′	0.4	$\gamma(C_3H)$ (26) + $\gamma(C_5H)$ (26) − $\gamma(C_2H)$ (10) − $\gamma(C_6H)$ (10)
18	1001	A″	0.0	$\beta_{2[NH2]}$ (23) − $\gamma(C_5H)$ (13) + $\gamma(C_3H)$ (13) −$\nu(C_1C_2)$ (13) + $\nu(C_1C_6)$ (13)
19	1068	A″	0.5	$\nu(C_4C_5)$ (32) − $\nu(C_3C_4)$ (32) − $\beta(C_4H)$ (18)
20	1147	A″	0.6	$\beta_{2[NH2]}$ (26) − $\beta(C_2H)$ (16) − $\beta(C_6H)$ (16) + $\beta(C_3H)$ (12) + $\beta(C_5H)$ (12)
21	1188	A′	1.3	$\beta(C_6H)$ (25) − $\beta(C_2H)$ (25) − $\beta(C_5H)$ (14) + $\beta(C_3H)$ (14)
22	1252	A′	4.4	$\nu(C_1N_7)$ (68)
23	1285	A″	0.4	$\beta(C_4H)$ (26) + $\beta_{2[NH2]}$ (17)
24	1354	A″	1.7	$\nu(C_4C_5)$ (13) − $\nu(C_3C_4)$ (13) − $\beta(C_5H)$ (11) − $\beta(C_3H)$ (11)
25	1378	A″	3.5	$\beta(C_4H)$ (17) + $\beta(C_3H)$ (16) + $\beta(C_5H)$ (16) − $\nu(C_1C_2)$ (12) + $\nu(C_1C_6)$ (12)
26	1440	A′	5.3	$\beta(C_3H)$ (22) − $\beta(C_5H)$ (22) − $\beta(C_6H)$ (17) + $\beta(C_2H)$ (17)
27	1538	A″	0.7	$\nu(C_2C_3)$ (26) − $\nu(C_5C_6)$ (26) − $\beta(C_4H)$ (19)
28	1595	A′	5.5	$\nu(C_5C_6)$ (29) + $\nu(C_2C_3)$ (29)
29	1618	A′	32.2	$\beta_{1[NH2]}$ (92)
30	3137	A′	5.8	$\nu(C_2H)$ (30) + $\nu(C_6H)$ (30) − $\nu(C_3H)$ (19) − $\nu(C_5H)$ (19)
31	3138	A″	0.3	$\nu(C_6H)$ (36) − $\nu(C_2H)$ (36) − $\nu(C_5H)$ (14) + $\nu(C_3H)$ (14)
32	3155	A′	7.5	$\nu(C_3H)$ (27) + $\nu(C_5H)$ (27) + $\nu(C_2H)$ (19) + $\nu(C_6H)$ (19)
33	3157	A″	48.0	$\nu(C_5H)$ (36) − $\nu(C_3H)$ (36) + $\nu(C_6H)$ (14) − $\nu(C_2H)$ (14)
34	3193	A′	13.3	$\nu(C_4H)$ (92)
35	3449	A′	32.9	$\nu(N_7H)$ (50) + $\nu(N_7H)$ (50)
36	3583	A′	3.4	$\nu(N_7H)$ (50) − $\nu(N_7H)$ (50)

[a] ν, stretching; β, bending; γ, out of plane; β_{1rg}, β_{2rg}, β_{3rg}, bending of six-membered ring; δ_{1rg}, δ_{2rg}, $\delta_{3rg,}$ δ_{4rg}, deformation of six-membered ring; $\tau_{[NH2]}$, torsion of NH_2.

similar hfcc values. The hfcc's in C_1, N_7, and hydrogen atoms connected with N_7 are obviously larger than the values in other atoms. The changes of bond distances in the T_1 and S_0 states can be explained by the changes of spin densities. For example, the spin density created on the C_1 atom following excitation to the T_1 state is obviously a factor leading to an increase of the C_1C_2 and C_1C_6 bond distances. The electronic distribution will be discussed in a following section.

3.3. Vibrational Frequencies. Table 4 records the fundamental vibrational frequencies and associated potential energy distribution (PED) of the T_1 aniline. The calculated values were obtained from scaled UB3LYP/6-311++G(3df,2p) harmonic frequencies. The nonredundant set of vibrations has been assigned using symmetrized internal coordinates, together with the associated PED's of calculated vibrational modes.[32]

The PED matrix is classically defined as PED $= \Lambda^{-1}\mathbf{JF}$, in which **F** stands for the harmonic force constants matrix in term of symmetrized internal coordinates, Λ represents the corresponding eigenvalue matrix, and finally **J** is the Jacobian matrix of Λ with respect to **F**. The normal modes of vibration are schematically illustrated in Figure 3. As far as we are aware, there is no experimental IR data for triplet aniline yet. The vibronic structure of phosphorescence bands was analyzed, but they are rather puzzling, strongly different from experiment conditions.[15]

The antisymmetrical (Q36) and symmetrical (Q35) stretching related to the NH_2 group modes positioned at 3449 and 3583 cm^{-1}, respectively. According to the calculated PED (Table 4), the NH_2 scissoring vibration contributes to a dominant contribution to Q29. The C−N stretching contributes predominantly to the mode Q22 (68%) whose frequency at 1252 cm^{-1} was obtained. The ν(C−N) stretch frequency is marginally smaller than that of 1293 cm^{-1} of aniline ground state. However, the corresponding IR intensity is much reduced in the high spin state. The modes associated with the phenyl ring vibrations are relatively less sensitive to the nature of the substituent. The five modes Q30−Q34 dominated by the C−H stretching combinations vibrate at the frequencies of 3193 cm^{-1} (Q34), 3157 cm^{-1} (Q33), 3138 cm^{-1} (Q32), and 3137 cm^{-1} (Q30; cf. Figure 3).

3.4. Electronic Distribution of the First Triplet Aniline. Figure 4 illustrates some aspects of the electronic distribution of the vertical triplet aniline, which is the triplet state initially formed at the singlet geometry. Figure 5 summarizes the electronic distribution of the adiabatic triplet aniline. The electronic distribution in ground state of aniline is illustrated in the electronic Supporting Information (Figure 2S). The density difference function whose map is presented in Figure 5a is defined by

$$\Delta\rho(\mathbf{r}) = \rho_{\text{vertical triplet}}(\mathbf{r}) - \rho_{\text{singlet}}(\mathbf{r})$$

It indicates how electrons are moving during the vertical excitation. Blue contours show the regions where electron depletion ($\rho_{\text{triplet}}(\mathbf{r}) < \rho_{\text{singlet}}(\mathbf{r})$) and pink contours indicate where electron concentration ($\rho_{\text{triplet}}(\mathbf{r}) > \rho_{\text{singlet}}(\mathbf{r})$) occurs during the process. Calculated natural charges concur with the picture

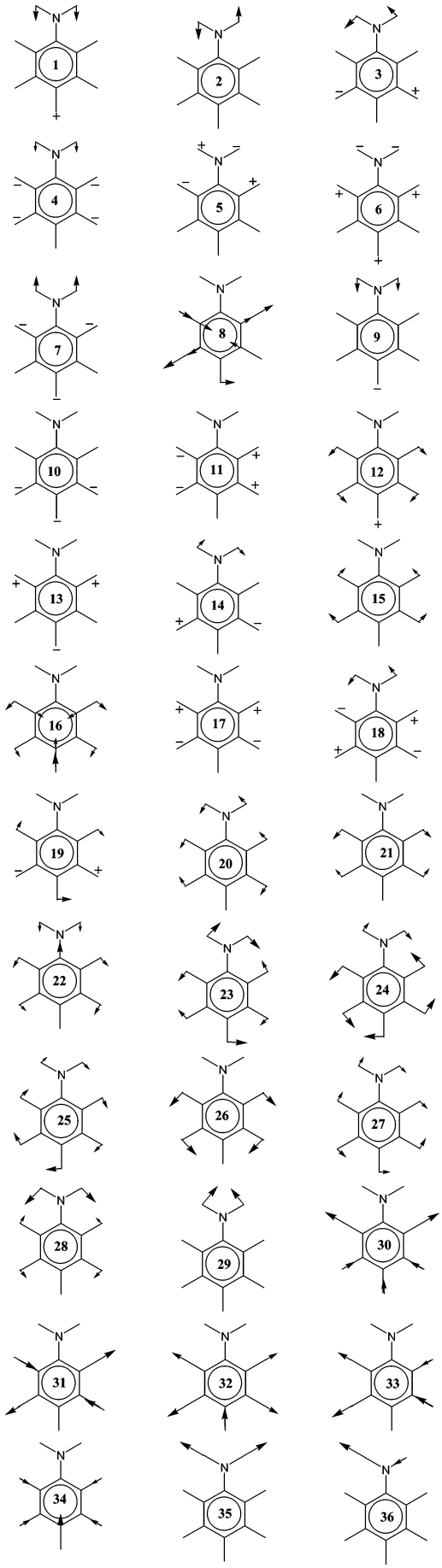

Figure 3. Normal displacements of the vibrational modes of the aniline triplet state. The B3LYP/6-311++G(3df,2p) method is employed. The assignments of the vibrational modes of the aniline triplet state are presented in Table 4.

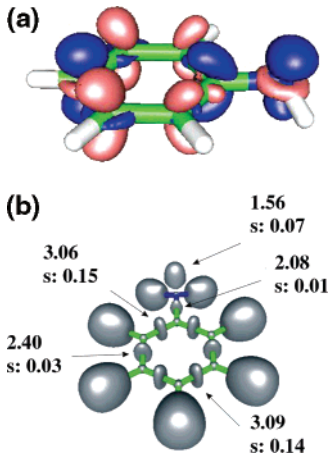

Figure 4. Aspects of the electronic distribution in the vertical triplet aniline (triplet state at singlet ground-state geometry): (a) density difference function, where pink represents the $\Delta\rho(\mathbf{r}) = 0.005$ au and blue represents the $\Delta\rho(\mathbf{r}) = -0.005$ au isosurface of the difference density; (b) ELF = 0.87 au isosurfaces of the electron localization function. Values are in atomic units and correspond to basin populations and integrated spin densities (*s* values).

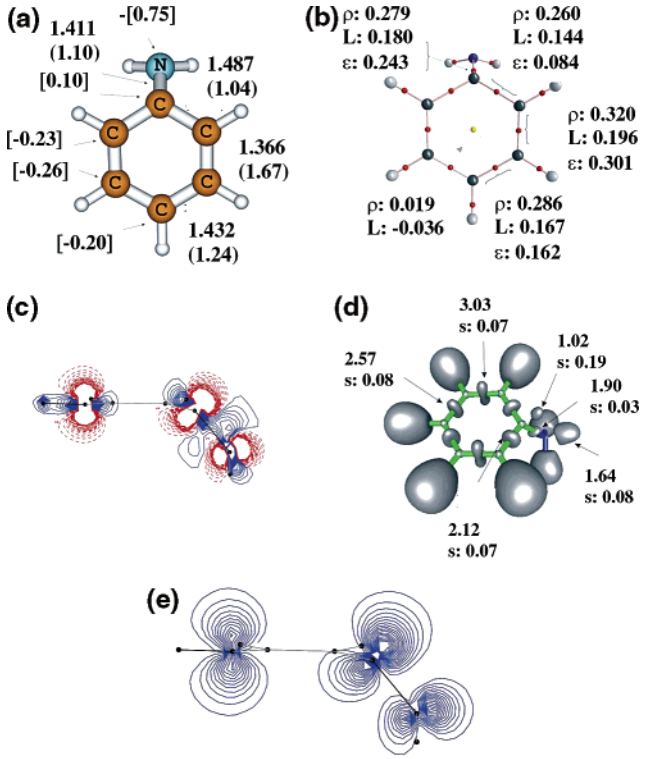

Figure 5. Summary of electronic distribution in triplet aniline: (a) bond distances (Å), NBO charges (brackets, in au), and Wiberg indices (parentheses, in au); (b) topology of the electron density determined from atom-in-molecule calculations with $\rho(\mathbf{r})$ = electron density (au), L = Laplacian of the density defined as $L(\mathbf{r}) = -\nabla^2\rho(\mathbf{r})$ (au), and ϵ = ellipticity of the bond critical point; (c) Laplacian map of the density; (d) isosurfaces of the electron localization function, ELF = 0.87 au, where the values are the populations of the valence basins (au).

suggested by the differential densities, as they amount to 0.31, −0.70, and −0.03 e for nitrogen, *ipso*-C, and *para*-C, respectively, whereas they are −0.35 and −0.37 e in the cases of *ortho*-C and *meta*-C atoms.

We have also calculated the electron localization function (ELF)[33] of the molecule. The ELF values are always in the [0;1] interval and are large where electrons are alone or form pairs with antiparallel spins (localized) and are small where electrons

form mainly parallel-spin pairs. This approach allows us to decompose the space into a number of basins, which represent the cores, chemical bonds, and lone pairs. Theory of ELF allows us to define the properties of ELF basins: integrated electron density over an ELF basin shows its population, while the integrated spin density measures its "radical population". In this article we discuss only the valence (bonding) and lone pair basins, because properties of core basins do not change during excitations. As suggested by the shape of the HOMO and LUMO of the singlet state, the populations of the $V(C_{ipso},C_{ortho})$ and $V(C_{meta},C_{para})$ basins are increased during vertical excitation, while that of $V(C_{ortho},C_{meta})$ decreases, which gives a reversed bond order distribution as compared to the ground state. The integrated spin density shows that the unpaired electrons are mainly located in $V(C_{ipso},C_{ortho})$ and $V(C_{meta},C_{para})$ basins. The electron localization function of the vertical triplet state points out that, during vertical excitation, the lone pair of nitrogen donates electrons to the ring; the sum of the V(C,C) basin populations is now 17.1 e, but it is only 16.8 e in the singlet state.

Following geometry relaxation to the adiabatic triplet position, the nitrogen atom is moving out of the ring plane (Figure 2), and a new lone pair type valence basin (with 1.02 e population) on *ipso*-C takes place from the excess electron of the ring. As it can be seen on the map of the Laplacian of the electron density (Figure 5c),[34] there is a remarkable electron concentration on this basin. According to the integrated spin density values (Figure 5b), the $V(C_{ipso})$ basin has the largest radical character, whereas the remaining radical electrons are nearly equally distributed on V(N), V(C,N), and V(C,C) basins (Figure 5d). This is reflected in the spin density in the symmetry plane perpendicular to the ring plane (Figure 5e). The population of the $V(C_{ipso},C_{ortho})$ basin decreases dramatically, in agreement with the Wiberg indices, and $\rho(\mathbf{r})$ and ϵ correspond to the values of a single bond; therefore, the *ipso*-C can be regarded as a sp^3 carbon with a radical on it. On the contrary the bond order of the *ortho*-C−*meta*-C bond actually increases. It is interesting however that according to the calculated nucleus independent chemical shift (NICS) value, the triplet aniline is antiaromatic (NICS is 8.75), while the singlet ground state is aromatic (NICS is −8.66). This is in line that HOMO is bonding respect to $C_{ipso}-C_{ortho}$ and $C_{meta}-C_{para}$, while LUMO is antibonding respect to $C_{ortho}-C_{meta}$.

In summary, relative to the ground state, the C−C bonds become weaker and the C−N stronger. The charge distribution is reorganized at the benefit of the *ortho* and *meta* ring carbons. The *ipso*- and *para*-carbon and nitrogen atoms experience electron depletion. The *ipso*-carbon enjoys an excess of α-spin electrons. For their parts, the topology and the electron localization function (ELF) of the T_1 aniline are not basically different from those of the singlet S_0 counterpart.

In benzene solution, the dipole moment has been measured to be $\mu(T_1) = 2.1 \pm 0.2$ D.[35] The dipole moment lies in the C−N axis. In the T_1 state, the molecule tends to have a more biradical nature, which may cause a smaller contribution to the charge transfer in the C−N direction. Upon excitation, the electron density on the N atom is transferred mostly to the ring carbon atoms; therefore the dipole moment change in the triplet state is primary determined by this actual transfer.[35]

3.5. Protonation of Aniline in the T_1 State. The geometries of T_1 aniline protonated at different positions, optimized at the UB3LYP/6-311++G(d,p) level, are shown in the electronic Supporting Information (Figure 3S). The protonated forms are denoted as molecule **P1**, **P2**, **P3**, **P4**, and **P5** for protonation that occurs at N, *ipso*-C_1, *ortho*-C_2, *meta*-C_3, and *para*-C_4 sites, respectively. The forms **P1** and **P2** have C_s symmetry with the $N_7C_1C_4$ plane as the symmetry plane. The forms **P3** and **P4** are also under C_s symmetry but with the phenyl ring plane. The form **P5** exhibits nonplanar geometry without symmetry with dihedral angles of $C_1C_2C_3C_4$ and $C_1C_6C_5C_4$ that are 6.6 and −33.8°, respectively.

The NH_2 group of the forms **P1** and **P2** is obviously moving away from phenyl ring, and the phenyl rings of molecule **P5** are seriously distorted, which causes them to be less stable than the forms **P3** and **P4**. There is an interesting phenomenon in that the protonated molecule, which is characterized by a longer C−N bond length, possesses a smaller proton affinity than the isomer having a shorter C−N bond length. The strength of the C−N bond seems to have a significant contribution to the stability of the protonated form.

Protonation of triplet aniline is calculated to occur preferentially at the *meta*-C_3 site. The corresponding proton affinity, $PA(C_3) = 243.0$ kcal/mol, is significantly larger than the PA's of 206.9, 216.5, 221.6, and 237.9 kcal/mol at the N, *ipso*-C_1, *para*-C_4, and *ortho*-C_2 sites, respectively. Thus, nitrogen becomes the least basic site in the triplet state. Note that, in the ground state, aniline protonation takes place at both N and *para*-C atoms, depending on the experiment conditions.[36] The calculated PA's at both sites are quite close to each other and also depend on the methods employed.[37]

4. Conclusions

In this theoretical study, accurate quantum chemical calculations were performed to provide a clear and detailed characterization of the triplet states of aniline. MS-CASPT2 based on CASSCF(10,12)/ANO calculations, including the Rydberg states, predicts the nature of a series of low-lying triplet states. Both the T_1 ($1^3A'$) and T_2 ($1^3A''$) states are found to be below the lowest-lying singlet S_1 ($1^1A''$) state. The first three triplet states and the T_5 state correspond to valence states whereas the T_4, T_6, and T_7 excited states are 3s-, $3p_y$-, and $3p_z$-Rydberg states, respectively. Geometry, vibrational modes, and electron distribution of the lowest lying T_1 ($1^3A'$) state have been determined using the UB3LYP method. T_1 aniline is no longer an aromatic molecule. The vertical and adiabatic singlet−triplet energy gaps $\Delta E(S_0-T_1)$ amount to 3.7 and 3.5 eV, respectively. In clear contrast with the S_0 state, protonation of T_1 aniline occurs preferentially at the ring *meta*-carbon site, with a proton affinity of PA = 243 kcal/mol, with a probably error of ±3 kcal/mol.

Acknowledgment. This work was carried out within the framework of a bilateral cooperation program between the Governments of Hungary and the Flemish Community of Belgium (Project BIL-01/17). The Leuven group is indebted to the K.U. Leuven Research Council for continuing support (GOA program).

Supporting Information Available: Figures showing CASSCF and B3LYP/6-311++G(d,p) optimized geometric parameters for aniline in the ground singlet state, a summary of the electronic distribution in aniline, and selected (U)B3LYP/6-311++G(d,p) geometrical parameters of protonated aniline in the lowest-lying triplet state. This material is available free of charge via the Internet at http://pubs.acs.org.

References and Notes

(1) (a) Merchan, M.; Serrano-Andres, L.; Robb, M. A.; Blancafort, L. *J. Am. Chem. Soc.* **2005**, *127*, 1820. (b) Cadet, J.; Vigny, P. In *Bioorganic*

Photochemistry; Morrison, H., Ed.; John Wiley & Sons: New York, 1990; Vol. 1, pp 1−272.

(2) (a) Douki, T.; Cadet, J. *Biochemistry* **2001**, *40*, 2495. (b) Douki, T.; Reynaud-Angelin, A.; Cadet, J.; Sage, E. *Biochemistry* **2003**, *42*, 9221.

(3) Blancafort, L.; Sodupe, M.; Bertran, J. *J. Am. Chem. Soc.* **2004**, *126*, 12770.

(4) Bent, D. V.; Hayon, E. *J. Am. Chem. Soc.* **1975**, *97*, 2599, 2606, and 2612.

(5) (a) Kimura, K.; Tsubomura, H.; Nagakura, S. *Bull. Chem. Soc. Jpn.* **1964**, *37*, 1336. (b) Kimura, K.; Nagakura, S. *Mol. Phys.* **1965**, *9*, 117.

(6) Leal, J. M.; Garcia, B. *Z. Phys. Chem. (Leipzig)* **1988**, *269*, 26.

(7) (a) Fuke, K.; Kaya, K. *Chem. Phys. Lett.* **1983**, *94*, 97. (b) Fuke, K.; Nagakura, S. *J. Mol. Spectrosc.* **1977**, *64*, 139.

(8) Bryce-Smith, D.; Gilbert, A. In *Rearrangement in Ground and Excited States*; Mayo, P. d., Ed.; Academic Press: New York, 1980; Vol. 3.

(9) Brand, J. C. D.; Williams, D. R.; Cook, T. J. *J. Mol. Spectrosc.* **1966**, *20*, 539.

(10) (a) Hollas, J. M.; Howson, M. R.; Ridley, T.; Halonen, L. *Chem. Phys. Lett.* **1983**, *98*, 611. (b) Bacon, A. R.; Hollas, J. M. *Faraday Discuss. Chem. Soc.* **1988**, *86*, 129. (c) Christofferson, J.; Hollas, J. M.; Kirby G. H. *Mol. Phys.* **1969**, *16*, 441.

(11) (a) Kerstel, E. R. Th.; Becucci, M.; Pietraperzia, G.; Consalvo, D.; Castellucci, E. *J. Mol. Spectrosc.* **1996**, *177*, 74. (b) Pietraperzia, G.; Becucci, M.; Del Pace, I.; Lopez-Tocon, I.; Castellucci, E. *Chem. Phys. Lett.* **2001**, *335*, 195.

(12) Hineman, M. F.; Kim, S. K.; Berstein, E. R.; Kelly, D. F. *J. Chem. Phys.* **1992**, *96*, 4904.

(13) Ebata, T.; Minejima, C.; Mikami, N. *J. Phys. Chem. A* **2002**, *106*, 11070.

(14) Honda, Y.; Hada, M.; Ehara, M.; Nakatsuji, H. *J. Chem. Phys.* **2002**, *117*, 2045.

(15) Gée, C.; Cuisset, A.; Divay, L.; Crepin, C. *J. Chem. Phys*. **2002**, *116*, 4993.

(16) Sarkar, S.; Kastha, G. *Spectrochim. Acta* **1992**, *48A*, 1611.

(17) Scheps, R.; Florida, D.; Rice, S. *J. Chem. Phys.* **1974**, *61*, 1730.

(18) (a) Hohenberg, P.; Kohn, W. *Phys. Rev. B* **1964**, *136*, 785. (b) Kohn, W.; Sham, L. J. *Phys. Rev. A* **1965**, *140*, 1133. (c) Becke, A. D. *J. Chem. Phys.* **1993**, *98*, 5648. (d) Lee, C.; Yang, W.; Parr, R. G. *Phys. Rev. B* **1988**, *37*, 785.

(19) (a) Roos, B. O.; Taylor, P. R.; Siegbahn, P. E. M. *Chem. Phys.* **1980**, *48*, 157. (b) Roos, B. O. In *Advances in Chemical Physics; Ab Initio Methods in Quantum Chemistry-II*; Lawley, K. P., Ed.; John Wiley & Sons Ltd.: Chichester, England, 1987; Chapter 69, p 399.

(20) (a) Andersson, K.; Malmqvist, P.-Å.; Roos, B. O.; Sadlej, A. J.; Wolinski, K. *J. Phys. Chem.* **1990**, *94*, 5483. (b) Andersson, K.; Malmqvist, P.-Å.; Roos, B. O. *J. Chem. Phys.* **1992**, *96*, 1218.

(21) (a) Andersson, K.; Malmqvist, P.-Å.; Roos, B. O. *J. Chem. Phys.* **1992**, *96*, 1218. (b) Finley, J.; Malmqvist, P. A.; Roos, B. O.; Serrano-Andres, L. *Chem. Phys. Lett.* **1998**, *288*, 299.

(22) Pierloot, K.; Dumez, B.; Widmark, P.-O.; Roos, B. O. *Theor. Chim. Acta* **1995**, *90*, 87.

(23) Frisch, M. J.; Trucks, G. W.; Schlegel, H. B.; Scuseria, G. E.; Robb, M. A.; Cheeseman, J. R.; Montgomery, J. A., Jr.; Vreven, T.; Kudin, K. N.; Burant, J. C.; Millam, J. M.; Iyengar, S. S.; Tomasi, J.; Barone, V.; Mennucci, B.; Cossi, M.; Scalmani, G.; Rega, N.; Petersson, G. A.; Nakatsuji, H.; Hada, M.; Ehara, M.; Toyota, K.; Fukuda, R.; Hasegawa, J.; Ishida, M.; Nakajima, T.; Honda, Y.; Kitao, O.; Nakai, H.; Klene, M.; Li, X.; Knox, J. E.; Hratchian, H. P.; Cross, J. B.; Bakken, V.; Adamo, C.; Jaramillo, J.; Gomperts, R.; Stratmann, R. E.; Yazyev, O.; Austin, A. J.; Cammi, R.; Pomelli, C.; Ochterski, J. W.; Ayala, P. Y.; Morokuma, K.; Voth, G. A.; Salvador, P.; Dannenberg, J. J.; Zakrzewski, V. G.; Dapprich, S.; Daniels, A. D.; Strain, M. C.; Farkas, O.; Malick, D. K.; Rabuck, A. D.; Raghavachari, K.; Foresman, J. B.; Ortiz, J. V.; Cui, Q.; Baboul, A. G.; Clifford, S.; Cioslowski, J.; Stefanov, B. B.; Liu, G.; Liashenko, A.; Piskorz, P.; Komaromi, I.; Martin, R. L.; Fox, D. J.; Keith, T.; Al-Laham, M. A.; Peng, C. Y.; Nanayakkara, A.; Challacombe, M.; Gill, P. M. W.; Johnson, B.; Chen, W.; Wong, M. W.; Gonzalez, C.; Pople, J. A. *Gaussian 03*, revision B.03; Gaussian, Inc.: Wallingford, CT, 2003.

(24) Andersson, K.; Fulscher, M. P.; Lindh, R.; Malmqvist, P.-Å; Olsen, J.; Sadlej, A. J.; Widmark, P.-O. *MOLCAS*, version 6.0; University of Lund: Lund, Sweden, 2004.

(25) Rubio-Pons, O.; Loboda, O.; Minaev, R.; Schimmelpfennig, B.; Vahtras O.; Agren, H. *Mol. Phys.* **2003**, *101*, 2103.

(26) Liu Y. J.; Persson P.; Lunell S. *J. Phys. Chem. A* **2004**, *108*, 2339.

(27) Hou X. J.; Nguyen M. T. Unpublished results.

(28) Swiderek P.; Michaud M.; Sanche L. J. *Chem. Phys.* **1996**, *105*, 6724.

(29) Hiraya A.; Shobatake K. *J. Chem. Phys.* **1991**, *94*, 7700.

(30) Nguyen, M. T.; Zhang, R.; Nam, P. C.; Ceulemans, A. *J. Phys. Chem. A* **2004**, *108*, 6554.

(31) Abouaf, R.; Pommier, J.; Dunet, H.; Quan, P.; Nam, P. C.; Nguyen, M. T. *J. Chem. Phys.* **2004**, *121*, 11668.

(32) Martin J. M. L.; Alsenoy Van C. *GAR2PED program*; University of Antwerpen: Antwerpen, Belgium, 1995.

(33) Becke, A. D.; Edgecombe, K. E. *J. Chem. Phys.* **1990**, *92*, 5397.

(34) Bader, R. F. W. *Atoms in Molecules. A Quantum Theory*; Clarendon: Oxford, U.K., 1990.

(35) Shimomori, H.; Sato, A. *J. Phys. Chem.* **1994**, *94*, 13481.

(36) Flammang, Dechamps, N.; Pascal, L.; Van Haverbeke, Y.; Berbaux, P.; Nam, P. C.; Nguyen, M. T. *Org. Chem. Lett.* **2004**, *1*, 21 and references therein.

(37) Le, H. T.; Flammang, R.; Barbieux-Flammang, M.; Gerbaux, P.; Nguyen, M. T. *Int. J. Mass Spectrom.* **2002**, *217*, 45 and references therein.